Importance of Coulomb correlation and spin-orbit coupling in a 5*d* pyrochlore: $Pr_2Ir_2O_7$

Sudhir K. Pandey and Kalobaran Maiti*
Department of Condensed Matter Physics and Materials Science, Tata Institute of Fundamental Research, Homi Bhabha Road, Colaba, Mumbai 400005, India

(Received 25 April 2010; revised manuscript received 17 June 2010; published 14 July 2010)

Employing state-of-the-art *ab initio* electronic band-structure calculations, we investigate the electronic structure of an interesting pyrochlore, $Pr_2Ir_2O_7$ exhibiting varied electronic and magnetic properties. The calculated results indicate that the derivation of the bulk properties requires consideration of spin-orbit coupling and finite on-site Coulomb interaction strength despite the fact that Ir 5*d* electronic states are expected to be highly extended. Ir 5*d* moment is found to be finite and couples ferromagnetically with the Pr 4*f* moments. The magnetic moment and the density of states at the Fermi level depend on the direction of magnetization considered in the calculations suggesting the highly anisotropic magnetic and electronic-transport behavior for this compound consistent with the experimental observations.

DOI: 10.1103/PhysRevB.82.035110 PACS number(s): 71.20.−b, 75.10.Lp, 71.27.+a

I. INTRODUCTION

Pyrochlores with general formula unit $A_2B_2O_7$ (*A* and *B* are metals, O represents oxygen) have attracted a great deal of attention due to the discovery of many interesting properties in these systems. In this structure (space group $Fd\bar{3}m$), *A* and *B* atoms form a cubic fcc lattice with an additional ordering along ⟨110⟩ direction as shown in Fig. 1. In the pyrochlore structure, all the tetrahedral sites occupied by the oxygen atoms are not equivalent: 48*f* sites have two *A* and two *B* neighbors, 8*b* sites have four *B* neighbors and 8*a* sites are vacant. Thus, *A* atoms have eight oxygen neighbors and *B* atoms form BO_6 octahedra, which are connected by corner sharing. Clearly, this structure is susceptible to geometrical frustration that may lead to many interesting electronic and magnetic properties in this class of systems.[1,2] However, most of the oxide pyrochlores studied show magnetic ordering[3] with some exceptions such as $Dy_2Ti_2O_7$ exhibiting spin ice behavior.[4] The magnetically ordered compounds are usually found to be ferromagnetic (FM) metals.[5–9]

Most of the pyrochlores studied are formed with rare-earth (*RE*) elements at *A* sites and 4*d*/5*d* transition metals (TMs) at *B* sites. The electronic and magnetic properties of these compounds are essentially determined by the localized *RE* 4*f* electrons forming local moments and itinerant TM 4*d*/5*d* electrons. It is already observed that electron-electron Coulomb repulsion (electron correlation) strength becomes weaker with the increase in the radial extension of the *d* orbitals.[10,11] Thus, the electron correlation strength among TM 5*d* electrons are expected to be weak.[12] However, some compounds exhibit signature of strong electron correlations, such as $Sm_2Mo_2O_7$ in its optical conductivity data.[6] $Y_2Ir_2O_7$ exhibits insulating behavior and their electronic-structure study show signature of strong electron correlation.[5,13] The magnetic ordering has also been observed to be produced by Ir 5*d* electrons in $A_2Ir_2O_7$ (*A*=Nd, Sm, and Eu).[9] Clearly the behavior of 5*d* electrons is quite complex.

The compound, $Pr_2Ir_2O_7$ is even more complex exhibiting plethora of interesting properties. It shows metallic behavior, does not show long-range magnetic order down to 120 mK unlike other Ir pyrochlores and exhibits a partial spin freezing at about 120 mK.[14–17] Magnetic-susceptibility data in the paramagnetic region indicates effective antiferromagnetic interaction between magnetic ions.[16] However, the magnetic susceptibility below 1.7 K shows ln(*T*) dependence and considered as a signature of ferromagnetic coupling responsible for the observed spin-liquid behavior.[17] Resistivity data below 50 K also revealed the ln(*T*) dependence that was interpreted in terms of Kondo effect.[16] The residual resistivity is found to be large (360 $\mu\Omega$ cm). The low-temperature Hall-effect measurements exhibit low-charge-carrier density at the Fermi level that may be one possible reason for the large residual resistivity.[16]

The magnetization measurements along [100], [110], and [111] at 70 mK have shown different values of magnetization.[16] Magnetic field dependent conductivity measurements have also indicated highly anisotropic electronic transport.[17] Hall resistivity data show anomalous Hall effect and interpreted in terms of spin chirality mechanism. Clearly, $Pr_2Ir_2O_7$ is an unusual compound possessing many interesting properties rarely found in other systems and naturally attracted significant attention.

In this paper, we present our results on the electronic band structure of $Pr_2Ir_2O_7$ obtained by *ab initio* electronic-structure calculations that helps to explore the origin of var-

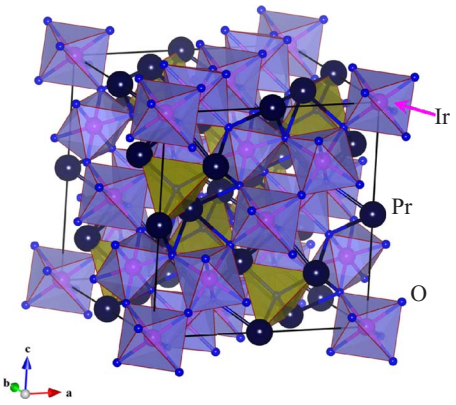

FIG. 1. (Color online) Crystal structure of $Pr_2Ir_2O_7$. The enclosed units are IrO_6 octahedra and OPr_4 tetrahedra.

ied interesting properties discussed above. These results indicate that the on-site Coulomb interaction and the spin-orbit coupling (SOC) are important to derive the electronic properties of this compound. Ir $5d$ moments couple ferromagnetically with the Pr $4f$ moments. Calculations for different magnetization directions reveal anisotropy in the density of states at the Fermi level that can directly be correlated with the experimentally observed anisotropy in the transport and magnetic properties.

II. COMPUTATIONAL DETAILS

The spin-unpolarized (nonmagnetic) and spin-polarized (magnetic) generalized gradient approximation (GGA) and GGA+U (U=on-site Coulomb interaction strength) electronic band-structure calculations were carried out employing *state-of-the art* full-potential linearized augmented plane-wave method using WIEN2K software.[18] The structural parameters used for the calculations are, $a=b=c=10.3995$ Å.[19] The crystal structure of $Pr_2Ir_2O_7$ is shown in Fig. 1, where Pr, Ir, and O atoms are denoted by spheres of decreasing size, respectively. In this structure, the oxygen atoms occupying 48f tetrahedral sites are denoted by O1 and the ones occupying 8b sites are denoted by O2. Pr and Ir atoms occupy 16c and 16d sites, respectively.[19] Therefore, Ir atoms are surrounded by six O1 atoms making an $IrO1_6$ octahedron and O2 is surrounded by four Pr atoms forming a tetrahedron. The muffin-tin sphere radii were chosen to be 1.95 a.u., 2.1 a.u., and 1.7 a.u. for Pr, Ir, and O atoms, respectively.

For the exchange-correlation functional, we adopted the GGA form of Perdew *et al.*[20] and the on-site Coulomb interaction was considered within the formulation of Anisimov *et al.*[21] The evolution of the electronic density of states was investigated by varying the on-site Coulomb interaction strength among Pr $4f$ electrons, U_{ff} and that among Ir $5d$ electrons, U_{dd}. The spin-orbit couplings for Pr and Ir atoms were also considered in the calculations. In order to capture anisotropy, calculations were carried out for different magnetization directions. The convergence was achieved by considering 512 k points within the first Brillouin zone. The error bar for the energy convergence was set to be smaller than 2.5×10^{-5} Ry/f.u. (f.u.=formula units) and the charge convergence was achieved to be less than 10^{-3} electronic charge in every case.

III. RESULTS AND DISCUSSIONS

A. Nonmagnetic and ferromagnetic solutions

The calculated partial density of states (PDOS) corresponding to the nonmagnetic GGA calculations are shown in Fig. 2. Pr $4f$ PDOS shown in Fig. 2(a) are mainly lying in the narrow energy range of −0.2 to 0.8 eV indicating highly localized nature of the $4f$ states. The energy bands representing O2 $2p$ PDOS appear primarily between −6.5 and −3.3 eV. In addition, O2 $2p$ PDOS contributions are also found in the energy range of −0.2 to 0.8 eV, where Pr $4f$ bands appear exhibiting similar symmetry of these two states due to finite hybridization as expected from the structure.

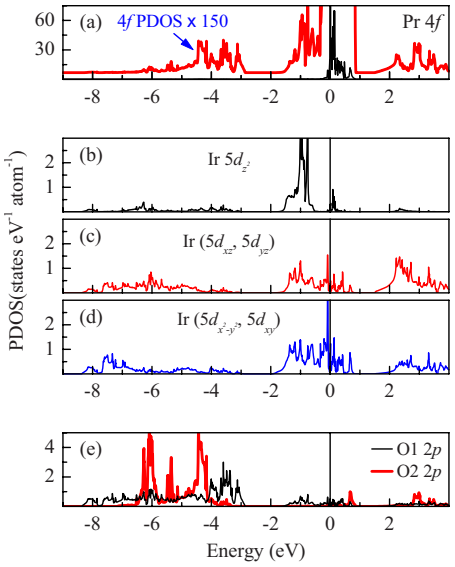

FIG. 2. (Color online) PDOS of (a) Pr $4f$ (thin line), (b) Ir $5d_{z^2}$ (c) Ir $(5d_{xz},5d_{yz})$, (d) Ir $(5d_{x^2-y^2},5d_{xy})$, and (e) O1 $2p$ and O2 $2p$ characters obtained from nonmagnetic GGA calculation. The thick solid line in (a) is the Pr $4f$ PDOS rescaled by 150 times and shifted along y axis.

This can be viewed clearly in the rescaled data shown in Fig. 2(a) (Pr $4f$ PDOS is multiplied by 150 and shifted along y axis in the figure). The relatively small contribution of O2 $2p$ states in the region of Pr $4f$ states and vice versa, presumably due to the large Pr-O2 bond distance (2.25 Å), is an indication of small overlap of these states that makes $4f$ states highly localized.

On the other hand, Ir $5d$ and O1 $2p$ states are spread over a relatively larger energy range showing extended nature of these states. From Figs. 2(b) and 2(c), it is clear that the shape and energy distribution of Ir $5d$ and O1 $2p$ PDOS are very similar indicating significant covalency[22] between them. The occupied Ir $5d$ PDOS can be divided into three regions. Region between −8.3 and −4.2 eV has highly mixed Ir $5d$ and O1 $2p$ character and is due to the bonding states. Region between −4.2 and −2.8 eV has dominating O1 $2p$ character, which corresponds to the nonbonding O1 $2p$ states. The energy region above −1.8 eV has dominating Ir $5d$ character with small contribution from O1 $2p$ states and is identified as antibonding bands.

In the coordinate system shown in Fig. 1, crystal field leads to a splitting of the fivefold-degenerate Ir $5d$ level into three levels consisting of d_{z^2}, (d_{xz},d_{yz}), and $(d_{x^2-y^2},d_{xy})$ orbitals. Such crystal-field splitting of Ir $5d$ bands can be seen clearly in Figs. 2(b)–2(d). It is to note here that Pr $4f$ PDOS also have finite contributions in these energy regions. This indicates finite hybridization between Ir $5d$ and Pr $4f$ electronic states. At the Fermi level, ϵ_F, the contribution from Pr $4f$ states are largest (~64 states/eV) with negligibly small contributions from Ir $5d$ (~0.8 states/eV) and O $2p$(~0.2 states/eV) states. Among the Ir $5d$ states, the contribution from d_{z^2} at ϵ_F is almost negligible.

Being identified the character of various energy bands in the electronic structure and the crystal-field splitting, we now

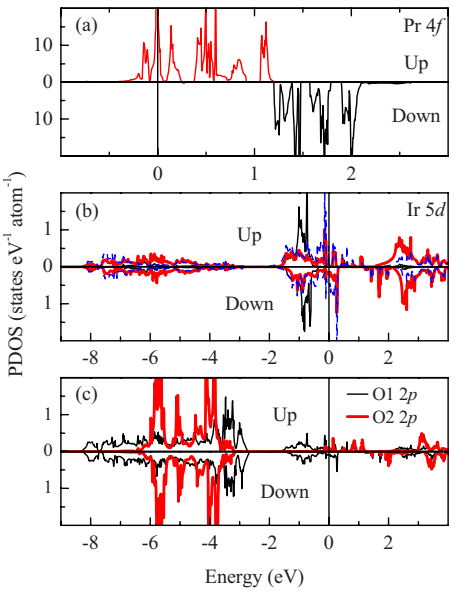

FIG. 3. (Color online) Partial density of states of (a) Pr $4f$, (b) Ir $5d$ having d_{z^2} (thin solid lines), (d_{xz},d_{yz}) (thick lines) and $(d_{x^2-y^2},d_{xy})$ (dashed lines), and (c) O1 $2p$ and O2 $2p$ characters obtained from ferromagnetic GGA calculations.

investigate the magnetic states of the Pr and Ir atoms in this compound. We have carried out the spin-polarized calculations for the FM arrangement of the magnetic moments. The total energy per formula unit for the FM solution is found to be about 1.222 eV less than that for nonmagnetic solution indicating that the ground state of $Pr_2Ir_2O_7$ should be magnetic within this local density-functional approach. The total magnetic moment per formula unit obtained from the calculation is about $4.38\mu_B$ with contributions from Pr and Ir atoms are about $1.78\mu_B$ and $0.2\mu_B$, respectively.

The PDOS of Pr $4f$, Ir $5d$, and O $2p$ characters corresponding to the FM solution are shown in Fig. 3. The Pr $4f$ states in the up-spin channel mainly lie between −0.4 and 1.2 eV and that in down-spin channel between 1.2 and 2.1 eV. The Pr $4f$ bands are fully spin polarized indicating the strong Hunds coupling between Pr $4f$ electrons. The exchange splitting of $4f$ level is found to be ~1.3 eV. In the occupied part of the electronic structure, the energy spread of Ir $5d$ and O $2p$ states are almost similar as observed in the nonmagnetic case. In the up-spin channel, there are large $4f$ PDOS (~22 states/eV) at ϵ_F whereas the contribution from the $5d$ states is negligibly small (~0.15 states/eV). In the down-spin channel only Ir $5d$(~0.65 states/eV) and O $2p$ states contribute at ϵ_F. Thus, the magnetic interactions reduce the Pr $4f$ PDOS at ϵ_F by about three times leaving the Ir $5d$ PDOS unchanged.

The presence of finite DOS at ϵ_F indicates the metallic ground state, which is in accordance with the experimental observation.[16] It is to note here that the GGA calculations do not capture the highly correlated Pr $4f$ states well and hence, the observation of large contribution of Pr $4f$ PDOS at ϵ_F needs careful considerations.[23] However, such density-functional calculations provide valuable information about the crystal-field energy and exchange energy of different orbitals.[24] In order to know the crystal-field splitting of the

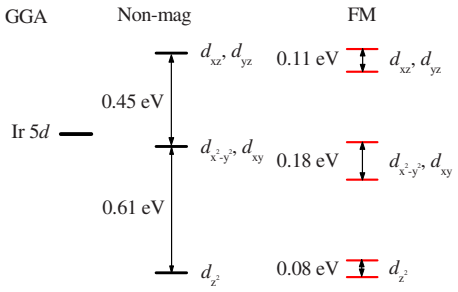

FIG. 4. (Color online) Schematic energy-level diagram of d_{z^2}, (d_{xz},d_{yz}), and $(d_{x^2-y^2},d_{xy})$ levels of Ir obtained from nonmagnetic and FM solutions.

Ir $5d$ orbitals, we have estimated the center of gravity of d_{z^2}, (d_{xz},d_{yz}), and $(d_{x^2-y^2},d_{xy})$ bands obtained from nonmagnetic calculations [see Fig. 2(b)]. The corresponding exchange splitting can be estimated from the center of gravity of the respective bands in up- and down-spin channels obtained from FM solution.

The energy-level diagrams exhibiting the crystal-field and exchange splitting are shown in Fig. 4. d_{z^2} states possess lowest energy and (d_{xz},d_{yz}) bands have highest energy. The separation between d_{z^2} and $(d_{x^2-y^2},d_{xy})$ levels is about 0.61 eV and that between $(d_{x^2-y^2},d_{xy})$ and (d_{xz},d_{yz}) levels is about 0.45 eV. The exchange splitting of d_{z^2}, $(d_{x^2-y^2},d_{xy})$, and (d_{xz},d_{yz}) bands are ~0.08 eV, 0.18 eV, and 0.11 eV, respectively, which are much smaller than that observed for $3d$ electronic states in $3d$ transition-metal oxides as expected due to the larger radial extension of the $5d$ orbitals compared to the $3d$ orbitals.[25]

B. Influence of spin-orbit interaction

$Pr_2Ir_2O_7$ contains heavier atoms such as Pr and Ir. Therefore, SOC strength is expected to be large and likely to play an important role in deciding the ground state of this compound. We have calculated the FM ground state, considering SOC for Pr and Ir electrons. The magnetization direction for the calculation is considered along [001]. The spin part of magnetic moment of Pr atom remains almost insensitive to the SOC, however, that of Ir atom reduces by $\sim 0.16\mu_B$. Total spin magnetic moment per formula unit is $\sim 3.75\mu_B$. The orbital magnetic moment for Pr atom is found to be about $-1.15\mu_B$ and that for Ir atom is $0.006\mu_B$. The negative sign of the orbital magnetic moment for Pr atom indicates that the direction of the orbital moment is opposite to the spin moment consistent with the Hund's rule for less than half-filled cases. The total magnetic moment (spin plus orbital part) per formula unit is $1.45\mu_B$.

In Fig. 5, we show the calculated PDOS, when spin-orbit coupling is considered. Due to the inclusion of SOC, Pr $4f$ PDOS become broader and their contribution at ϵ_F reduces by about four times. Comparison of Figs. 3 and 5 indicates that the SOC influences the energy distribution of Ir $5d$ electronic states too. In Fig. 3(b), the d_{z^2} orbital contributes primarily in the energy region of −1 to −0.5 eV. Around ϵ_F, the contribution from $(d_{x^2-y^2},d_{xy})$ orbitals is most significant among all the Ir $5d$ states. The SOC reduces the spectral

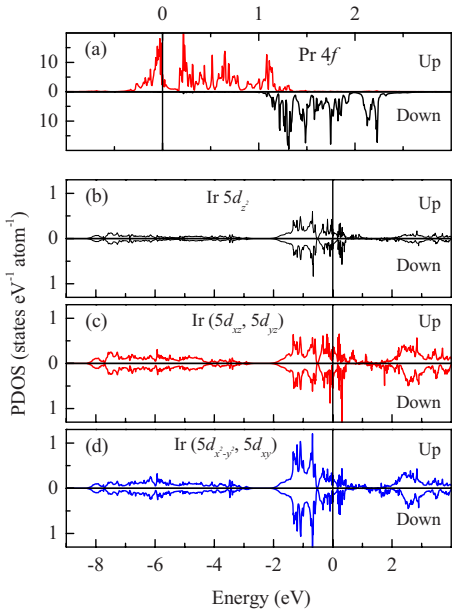

FIG. 5. (Color online) Partial density of states of (a) Pr $4f$ and (b) Ir $5d_{z^2}$ (c) Ir$(5d_{xz},5d_{yz})$, and (d) Ir$(5d_{x^2-y^2},5d_{xy})$ characters obtained from ferromagnetic GGA+SOC calculation. The up- and down-spin contributions are shown by positive and inverse y axis, respectively.

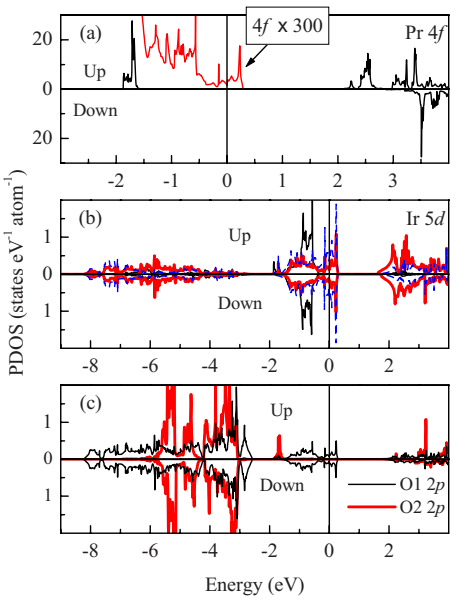

FIG. 6. (Color online) Partial density of states of (a) Pr $4f$, (b) Ir $5d$ having d_{z^2} (thin solid lines), (d_{xz},d_{yz}) (thick lines) and $(d_{x^2-y^2},d_{xy})$ (dashed lines) characters, and (c) O1 $2p$ and O2 $2p$ obtained from ferromagnetic GGA+U (U_{ff}=5 eV) calculation.

weight of $(d_{x^2-y^2},d_{xy})$ bands at ϵ_F by transferring the spectral weight to the energy region of −1.5 to −0.6 eV (see Fig. 5). Interestingly, SOC populates the Ir $5d$ states at the ϵ_F in the up-spin channel. However, Ir $5d$ contributions still remain smaller than Pr $4f$ contributions at ϵ_F indicating major role of Pr $4f$ states in the electronic properties.

C. Role of electron correlation

In order to investigate the role of electron-electron Coulomb repulsion in the electronic structure, we employed GGA+U method.[26] We calculated the FM ground states considering U_{ff} (electron correlation strength among Pr $4f$ electrons) =4 and 5 eV. U_{ff}=4 eV corresponds to an increment of the value of Pr magnetic moment by $0.11\mu_B$. Further increase in U_{ff} does not have significant effect on Pr magnetic moment. Interestingly, finite U_{ff} leads to a reduction in Ir magnetic moment by about $0.19\mu_B$ making it almost nonmagnetic. The total magnetic moments per formula unit comes out to be $\sim 4\mu_B$.

In Fig. 6, we show the calculated PDOS corresponding to U_{ff}=5 eV. Pr $4f$ up-spin bands split into two sets of bands; may be termed as lower and upper Hubbard bands separated by an energy gap of about 3.8 eV. The down-spin levels are completely unoccupied. The increase in U_{ff} enhances this gap keeping overall features of the PDOS very similar. Therefore, in the rest of the discussion, we have presented the results for U_{ff}=5 eV.

The effect of U_{ff} on Ir $5d$ and O $2p$ states far away from ϵ_F is not significant. The Ir $5d$ states in the vicinity of ϵ_F is, however, modified due to the finite U_{ff} as shown in Fig. 6(b). The finite exchange splitting seen by relative energy shift of the spin-up and spin-down Ir $5d$ PDOS in Fig. 3(b) is almost vanished in GGA+U results making Ir atom nonmagnetic as also reflected in the magnetic moment discussed above. Interestingly, the Ir $5d$ and O $2p$ PDOS between 0.3 and 1.6 eV seen in the up-spin channel in GGA calculation are absent in GGA+U calculations. In this energy range one can see the absence of Pr $4f$ states too. Appreciable Ir $5d$ and O2 $2p$ PDOS appear in the energy range between −1.9 and −1.6 eV, where Pr $4f$ states also contribute due to electron-correlation-induced energy shift. Evidently, such Ir $5d$ PDOS redistribution is linked to the change in Pr $4f$ PDOS indicating finite Ir $5d$-Pr $4f$ coupling as also manifested in Fig. 2. Parallel alignment of the Ir and Pr spin moments indicates ferromagnetic interaction between Pr $4f$ and Ir $5d$ spins. To check this result, we performed a calculation by considering the antiferromagnetic alignment of Pr $4f$ and Ir $5d$ spins as a starting point. The final self-consistent calculation converges to a ferromagnetic solution; Ir and Pr magnetic moments are aligned in the same direction.

The inclusion of U_{ff} in the calculation provides valuable insight about the nature of interaction between Pr $4f$ and Ir $5d$ electrons keeping the experimentally observed metallic ground state unchanged. The contribution of Pr $4f$ states at ϵ_F is negligibly small (~0.006 states/eV) as shown in zoomed scale in Fig. 6(a). Presence of large Ir $5d$ PDOS (~0.5 states/eV and 0.8 states/eV in up- and down-spin channels, respectively) suggests that the electronic transport in this compound is essentially determined by the Ir $5d$ electrons. The value of Ir $5d$ PDOS close to ϵ_F is comparable with that of the normal metals suggesting large charge-carrier density in $Pr_2Ir_2O_7$. However, the Hall measurements have shown that the carrier density of this compound is about 100 times smaller than that of normal metals.[16] It is important to note that the inclusion of SOC alone does not improve the situation significantly suggesting involvement of other parameters.

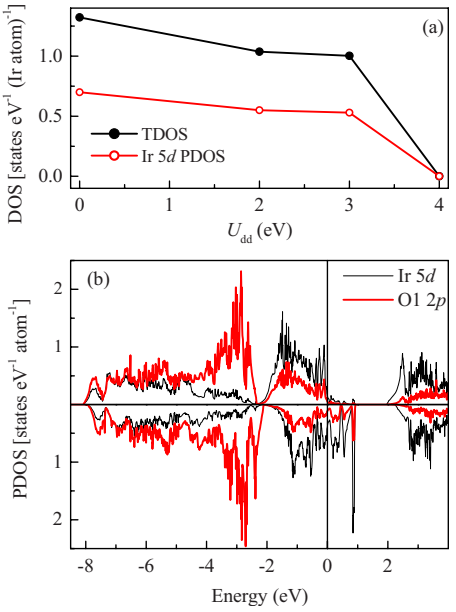

FIG. 7. (Color online) (a) TDOS and Ir 5d PDOS obtained from GGA+U+SOC calculations for different values of U_{dd} when U_{ff}=5 eV. (b) Ir 5d and O1 2p PDOS obtained from GGA+U+SOC (U_{ff}=5 and U_{dd}=3 eV) calculation.

D. Importance of both electron correlation and spin-orbit coupling

The contribution of the Ir 5d PDOS near ϵ_F can be influenced by the on-site Coulomb correlation among Ir 5d electrons, U_{dd}, which is underestimated in the calculations presented so far. While the electron correlation among Ir 5d electros, U_{dd} is expected to be less important due to large radial extension, a recent photoemission study on $Y_2Ir_2O_7$ and subsequent band-structure calculations have shown evidence of strong electron correlation among the Ir 5d electrons.[5,13] Thus, we calculated PDOS by varying U_{dd} from 2 to 4 eV in $Pr_2Ir_2O_7$. The total DOS and Ir 5d PDOS at the ϵ_F for varying U_{dd}(U_{ff}=5 eV) is shown in Fig. 7(a). It is evident from the figure that DOS at the ϵ_F decrease slowly with increase in U_{dd} up to 3 eV. For higher U_{dd}(=4 eV), DOS at ϵ_F become zero leading to opening of a hard band gap of ~0.26 eV that suggests a metal to insulator transition. Thus, on-site Coulomb interaction among Ir 5d electrons seems to have significant role in deriving the electronic properties of this compound and presumably responsible for the experimentally observed low carrier density in $Pr_2Ir_2O_7$.

Ir 5d and O1 2p states have been seen to be affected most by finite U_{dd}. We have shown the PDOS of Ir 5d and O1 2p states obtained from GGA+U+SOC (U_{ff}=5 and U_{dd}=3 eV) calculation in Fig. 7(b). Interestingly, PDOS appear to be almost half metallicle, as the DOS above ϵ_F is negligibly small in the up-spin channel in comparison to down-spin channel. The gap between the bands in the antibonding and nonbonding regions seen in Fig. 6(b) closes as U_{dd} transfers spectral weight of the antibonding Ir 5d bands toward higher binding energies and nonbonding O1 2p band shifts ~0.5 eV closer toward ϵ_F. The PDOS near the ϵ_F has dominating (d_{xz},d_{yz}) character.

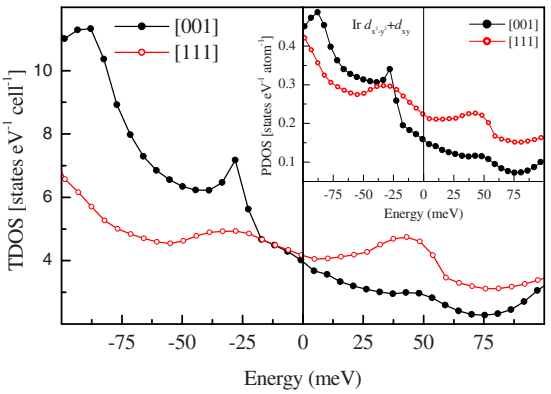

FIG. 8. (Color online) TDOS obtained from GGA+U+SOC (U_{ff}=5 and U_{dd}=3 eV) calculations keeping magnetization direction along [001] and [111]. Inset shows Ir($5d_{x^2-y^2}$,d_{xy}) PDOS.

The total occupancy of Ir 5d states is found to be 5.33, which is 0.33 more than the nominal occupancy of 5 for Ir in 4+ ionic state. This indicates the transfer of 0.33 electron from O1 2p orbital to Ir 5d orbital due to the hybridization. The total occupancy of Pr 4f orbital is 1.95, which is closer to the nominal occupancy of 2 for Pr^{3+} ion. The spin part of magnetic moments for Pr and Ir atoms are found to be ~1.9μ_B and 0.5μ_B, respectively. Thus, the U_{dd}=3 eV induces a magnetic moment of ~0.5μ_B at Ir site without changing the magnetic moment of Pr atom. The orbital part of magnetic moments for Pr and Ir atoms obtained from the calculation are ~−1.19μ_B and 0.21μ_B, respectively. If we compare the values of magnetic moments obtained from GGA+SOC calculation as mentioned earlier, we find that the orbital moment for Pr is not much influenced by U_{ff}. However, orbital moment for Ir is seen to be very much sensitive to U_{dd}; it increases with the increase in U_{dd}. The total magnetic moment (orbital plus spin part) per formula unit obtained for U_{ff}=5 and U_{dd}=3 eV is ~3.74μ_B.

Above results clearly establish the importance of Coulomb correlation and spin-orbit coupling in deriving the electronic and magnetic properties of this system. Presence of large orbital moment for Pr can lead to magnetic anisotropy. Moreover, the presence of correlation-induced orbital moment can also give rise to anisotropic electronic transport. To explore such possibility, we have calculated the ground-state energy and DOS by considering magnetization direction along [001] and [111]. The spin moment remains almost the same in both the cases. However, the orbital moments for Pr atoms are found to be very different. For example, the orbital moment for Pr atom situated at (0.5, 0.5, 0.5) position in the unit cell is found to be about −2.8μ_B and rest of the Pr atoms has the magnetic moment of about −0.9μ_B. The energy for [111] direction is found to be ~538 meV/fu less than that for [001] direction suggesting an easy axis of the magnetic moment to be along [111] direction. These results clearly indicate that the strong SOC of Pr 4f electrons is the primary cause for the experimentally observed magnetic anisotropy.

Total density of states (TDOS) in the vicinity of the Fermi level obtained for [001] and [111] directions are shown in Fig. 8. Inset shows the Ir($5d_{x^2-y^2}$,$5d_{xy}$) PDOS. It is evident from the figure that the density of states are very much sen-

sitive to the direction of the magnetization axis suggesting the anisotropic electronic transport as seen experimentally by Hall measurements.[17] At lower energies, TDOS corresponding to [001] is larger than that for [111] and crossover occurs at about −15 meV. Interestingly, TDOS within 25 meV of the Fermi level show quite different behavior. For the magnetization direction along [001] axis, TDOS decrease monotonically whereas that along [111] axis results to a nonmonotonic and almost symmetric DOS about the Fermi level, seems like a pseudogap. Present study suggests that at lower temperatures, the resistivity should decrease with the increase in temperature as carrier density increases with increase in temperature. This behavior is consistent with the experimental observation.[17]

IV. CONCLUSIONS

In conclusion, we studied the electronic structure of $Pr_2Ir_2O_7$ using *ab initio* electronic band-structure calculations within GGA and GGA+U formulations of density-functional theory. The results reveal that the spin-orbit coupling and the Coulomb correlation play important role in deriving the electronic structure of this compound. Ir 5d moment is found to be finite and couples ferromagnetically with the Pr 4f moment. The electronic states in the vicinity of the Fermi level and the Pr magnetic moment depend on the direction of magnetization considered in GGA+U+SOC calculations. These results explain the anisotropy observed in the electronic and magnetic properties.

*kbmaiti@tifr.res.in

[1] A. P. Ramirez, A. Hayashi, R. J. Cava, R. Siddharthan, and B. S. Shastry, Nature (London) **399**, 333 (1999).

[2] P. Schiffer, Nature (London) **420**, 35 (2002).

[3] M. A. Subramanian, G. Aravamudan, and G. V. Subba Rao, Prog. Solid State Chem. **15**, 55 (1983).

[4] J. Snyder, J. S. Slusky, R. J. Cava, and P. Schiffer, Nature (London) **413**, 48 (2001).

[5] R. S. Singh, V. R. R. Medicherla, K. Maiti, and E. V. Sampathkumaran, Phys. Rev. B **77**, 201102(R) (2008).

[6] Y. Yasui, Y. Kondo, M. Kanada, M. Ito, H. Harashina, M. Sato, and K. Kakurai, J. Phys. Soc. Jpn. **70**, 284 (2001).

[7] Y. Taguchi, K. Ohgushi, and Y. Tokura, Phys. Rev. B **65**, 115102 (2002).

[8] J. A. Hodges, P. Bonville, A. Forget, J. P. Sanchez, P. Vulliet, M. Rams, and K. Królas, Eur. Phys. J. B **33**, 173 (2003).

[9] K. Matsuhira, M. Wakeshima, R. Nakanishi, T. Yamada, A. Nakamura, W. Kawano, S. Takagi, and Y. Hinatsu, J. Phys. Soc. Jpn. **76**, 043706 (2007).

[10] M. Takizawa, D. Toyota, H. Wadati, A. Chikamatsu, H. Kumigashira, A. Fujimori, M. Oshima, Z. Fang, M. Lippmaa, M. Kawasaki, and H. Koinuma, Phys. Rev. B **72**, 060404(R) (2005); K. Maiti and R. S. Singh, *ibid.* **71**, 161102(R) (2005).

[11] K. Maiti, R. S. Singh, and V. R. R. Medicherla, Phys. Rev. B **76**, 165128 (2007); K. Maiti, *ibid.* **77**, 212407 (2008).

[12] K. Maiti, R. S. Singh, V. R. R. Medicherla, S. Rayaprol, and E. V. Sampathkumaran, Phys. Rev. Lett. **95**, 016404 (2005); K. Maiti, Phys. Rev. B **73**, 115119 (2006).

[13] K. Maiti, Solid State Commun. **149**, 1351 (2009).

[14] D. Yanagishima and Y. Maeno, J. Phys. Soc. Jpn. **70**, 2880 (2001).

[15] Y. Machida, S. Nakatsuji, H. Tonomura, T. Tayama, T. Sakakibara, J. van Duijn, C. Broholm, and Y. Maeno, J. Phys. Chem. Solids **66**, 1435 (2005).

[16] S. Nakatsuji, Y. Machida, Y. Maeno, T. Tayama, T. Sakakibara, J. van Duijn, L. Balicas, J. N. Millican, R. T. Macaluso, and J. Y. Chan, Phys. Rev. Lett. **96**, 087204 (2006).

[17] Y. Machida, S. Nakatsuji, Y. Maeno, T. Tayama, T. Sakakibara, and S. Onoda, Phys. Rev. Lett. **98**, 057203 (2007).

[18] P. Blaha, K. Schwarz, G. K. H. Madsen, D. Kvasnicka, and J. Luitz, in *Wien2k: An Augmented Plane Wave Plus Local Orbitals Program for Calculating Crystal Properties*, edited by K. Schwarz (Technische Universität Wien, Austria, 2001).

[19] J. N. Millican, R. T. Macaluso, S. Nakatsuji, Y. Machida, Y. Maeno, and J. Y. Chan, Mater. Res. Bull. **42**, 928 (2007).

[20] J. P. Perdew, K. Burke, and M. Ernzerhof, Phys. Rev. Lett. **77**, 3865 (1996).

[21] V. I. Anisimov, I. V. Solovyev, M. A. Korotin, M. T. Czyżyk, and G. A. Sawatzky, Phys. Rev. B **48**, 16929 (1993).

[22] E. Pavarini, S. Biermann, A. Poteryaev, A. I. Lichtenstein, A. Georges, and O. K. Andersen, Phys. Rev. Lett. **92**, 176403 (2004); E. Pavarini, A. Yamasaki, J. Nuss, and O. K. Andersen, New J. Phys. **7**, 188 (2005); K. Maiti, Phys. Rev. B **73**, 235110 (2006)

[23] V. I. Anisimov, A. I. Poteryaev, M. A. Korotin, A. O. Anokhin, and G. Kotliar, J. Phys.: Condens. Matter **9**, 7359 (1997); A. I. Lichtenstein and M. I. Katsnelson, Phys. Rev. B **57**, 6884 (1998); G. Kotliar, S. Y. Savrasov, K. Haule, V. S. Oudovenko, O. Parcollet, and C. A. Marianetti, Rev. Mod. Phys. **78**, 865 (2006).

[24] S. Patil, S. K. Pandey, V. R. R. Medicherla, R. S. Singh, R. Bindu, E. V. Sampathkumaran, and K. Maiti, J. Phys.: Condens. Matter **22**, 255602 (2010).

[25] Z. Y. Wu, M. Benfatto, M. Pedio, R. Cimino, S. Mobilio, S. R. Barman, K. Maiti, and D. D. Sarma, Phys. Rev. B **56**, 2228 (1997); S. K. Pandey, A. Kumar, S. Patil, V. R. R. Medicherla, R. S. Singh, K. Maiti, D. Prabhakaran, A. T. Boothroyd, and A. V. Pimpale, *ibid.* **77**, 045123 (2008); S. K. Pandey, S. Patil, V. R. R. Medicherla, R. S. Singh, and K. Maiti, *ibid.* **77**, 115137 (2008).

[26] V. I. Anisimov, F. Aryasetiawan, and A. I. Lichtenstein, J. Phys.: Condens. Matter **9**, 767 (1997).